Supporting Information

pH and Amphiphilic Structure Direct Supramolecular Behavior in Biofunctional Assemblies

Tyson J. Moyer,[‡] Joel A. Finbloom,[‡] Feng Chen, Daniel J. Toft, Vincent L. Cryns,* Samuel I. Stupp*

Supporting Figures

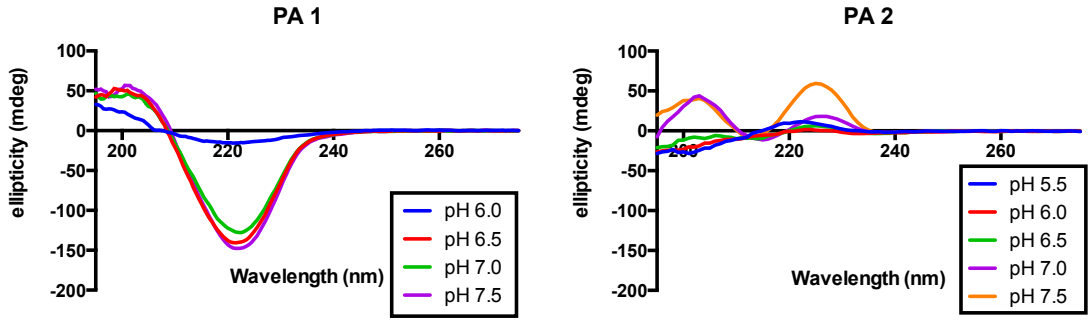

Figure 1S. Circular dichroism (CD) of PAs **1** and **2**. A pH-dependent decrease in CD signal was observed for both PAs **1** and **2**.

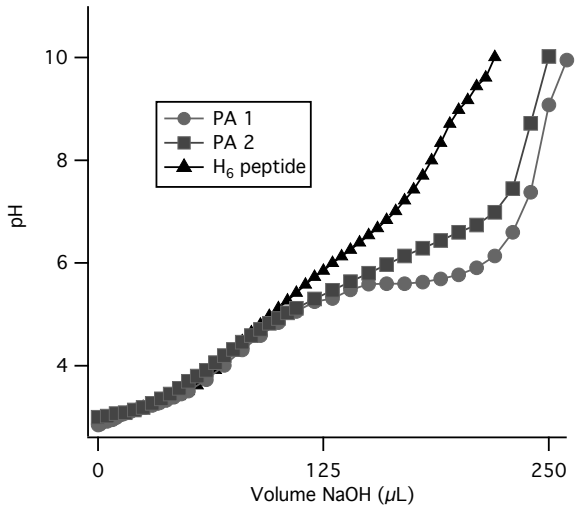

Figure 2S. Titration studies of PAs **1** (circles), **2** (squares), and Acet-H_6-NH_2 (triangles). Both PAs showed buffering capacities between pH 5.5 and 6.5, confirming the pH range observed for morphological changes in the PA assembly. For comparison, the H_6 peptide without an alkyl tail showed a lower buffering capacity relative to the assembled peptides.

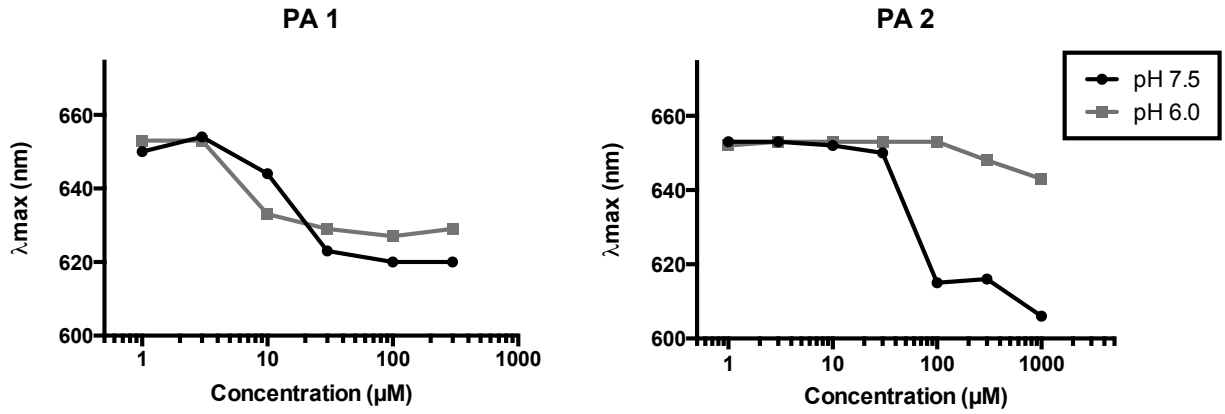

Figure 3S. Critical aggregation concentration (CAC) studies of PAs **1** and **2**. While both PAs showed more dramatic aggregation at pH 7.5 than pH 6.0, no significant shift in λ_{max} was observed at pH 6.0 for PA **2**.

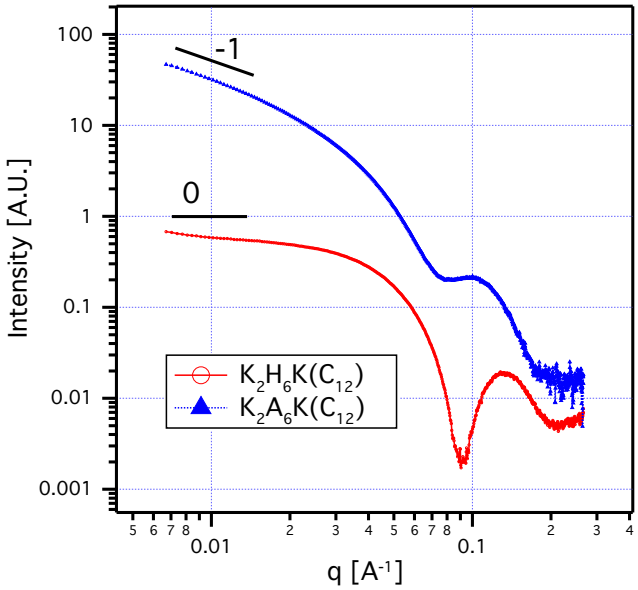

Figure 4S. SAXS of reverse histidine-based β-sheet PA, $K_2H_6K(C_{12})$, and reverse PA with a β-sheet region previous used previously, $K_2A_6K(C_{12})$, at pH 7.5. Reverse H_6 PA assembled into spherical micelles, while the reverse A_6 PA assembled into nanofibers.

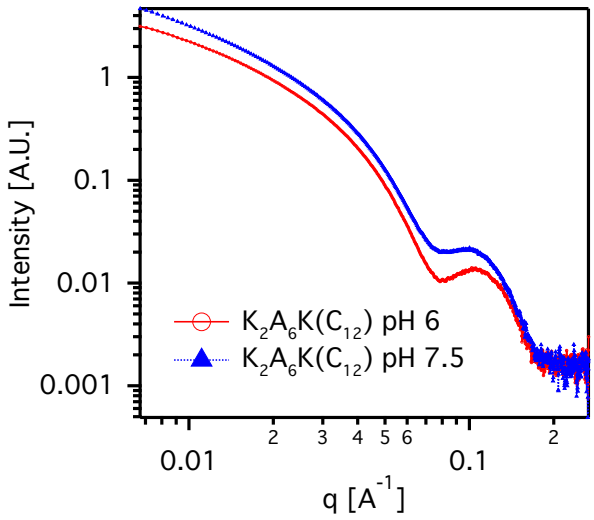

Figure 5S. SAXS of $K_2A_6K(C_{12})$ shows that A_6-based PAs do not show the same pH-dependent behavior found in the H_6-based PAs, and form cylinders at both acidic pH and physiological pH.

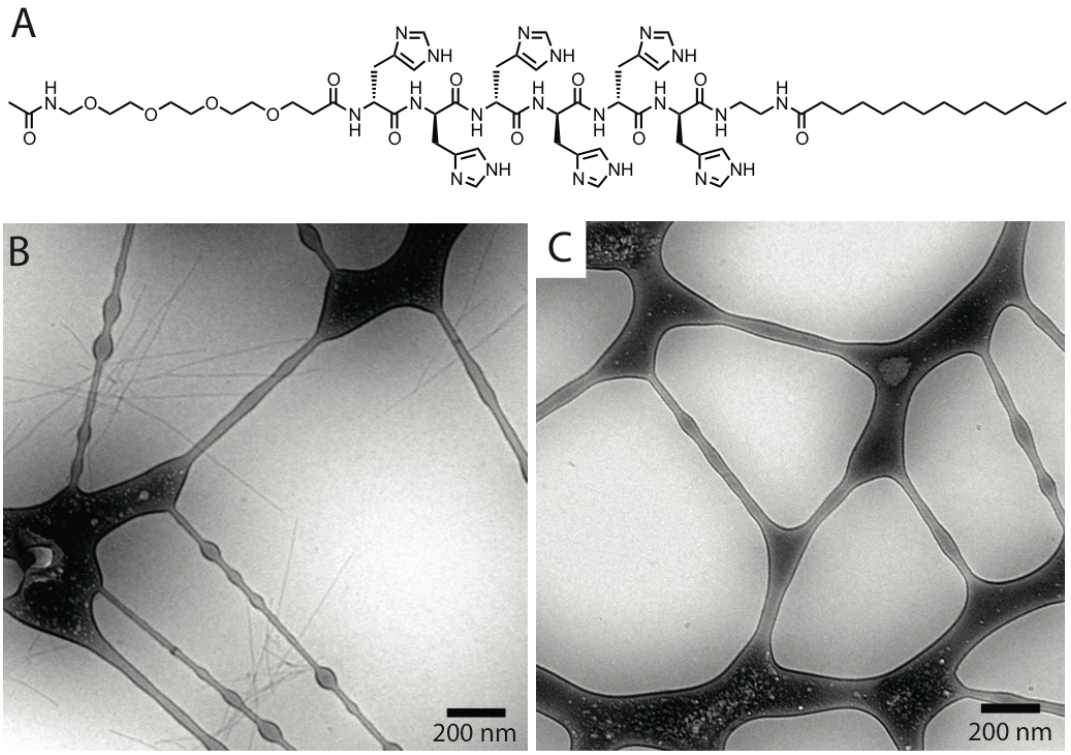

Figure 6S. (A) The chemical structure of Nova PA analogue to PA **2** shows a PA with the hydrophobic tail at the c-terminus, but without the side group of amide to disrupt hydrogen bonding. Myristic acid was used instead of dodecanoic acid because the carbon linker is shorter than the lysine side-chain. (B) At pH 7.5, this PA forms fibrous nanostructures by cryo-TEM. (C) At pH 6.0, nanostructures were not observed. For synthesis of this PA, a universal novatag resin was used. The mmt group was first deprotected off resin using 2% TFA, 5% TIPS, 93% DCM, and followed by a peptide coupling with myristic acid. Standard Fmoc-peptide synthesis was used for the remainder of the peptide, which was purified by HPLC.

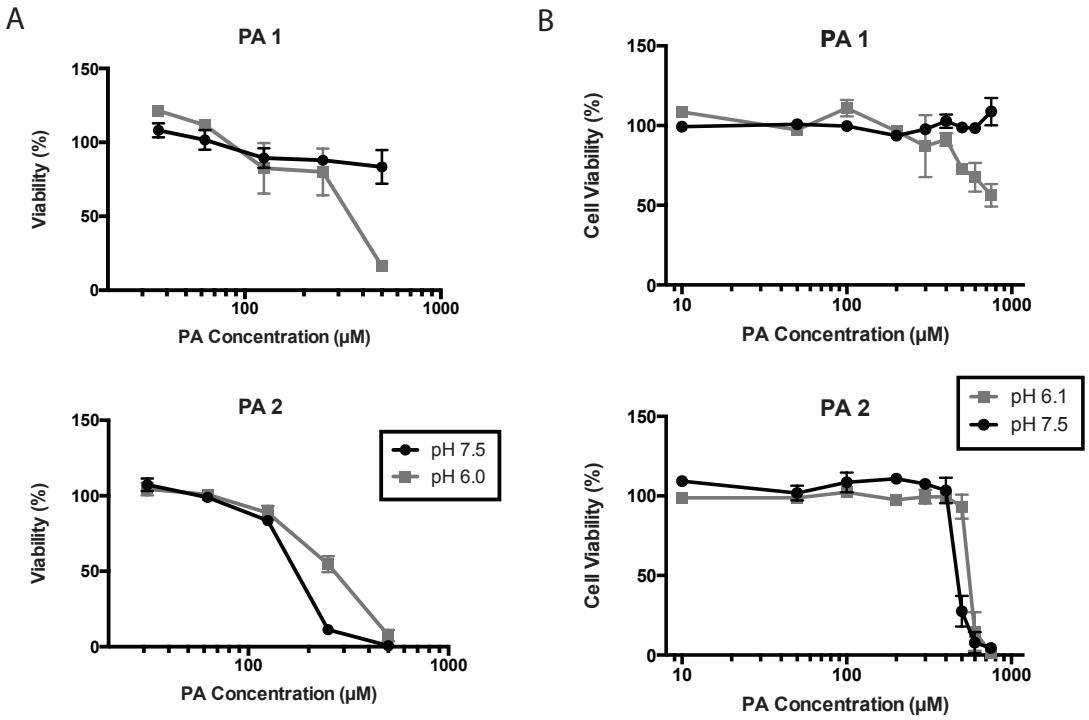

Figure 7S. MDA-MB 231 breast cancer cell viability at earlier passage (A) and later passage (B) shows the effect of passage number on nanostructure cytotoxicity.

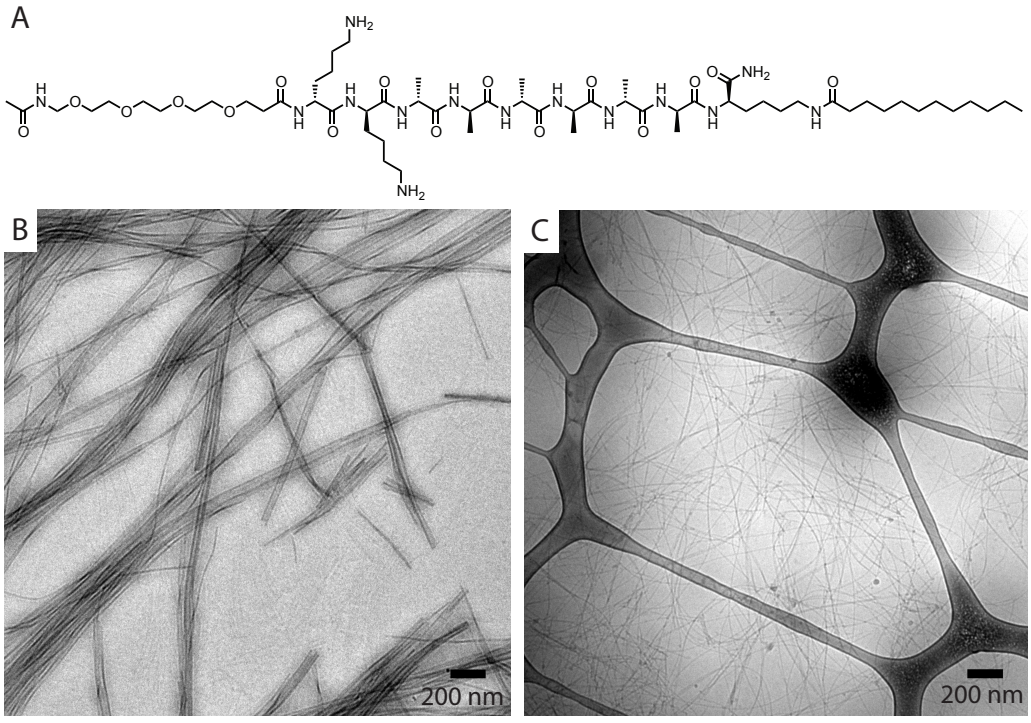

Figure 8S. (A) Chemical structure of the OEG-$K_2A_6K(C_{12})$ PA used for in vivo experiments. Cryo-TEM of $K_2A_6K(C_{12})$ PA at pH 7.5 PBS (B) and pH 6.0 PBS (C) show one-dimensional structures in both cases.

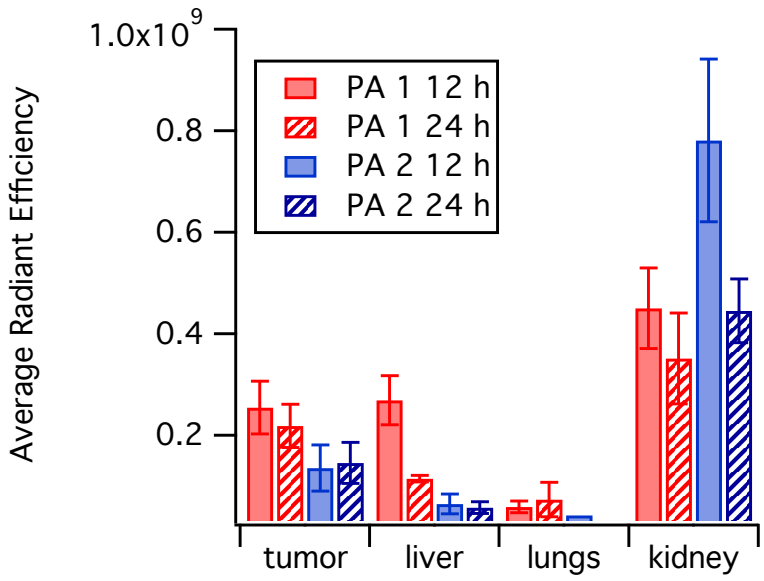

Figure 9S. Biodistribution of PAs **1** and **2** at 12 h and 24 h. Significant decreases in fluorescence of the liver for PA **1** and of the kidneys for PA 2 were observed.

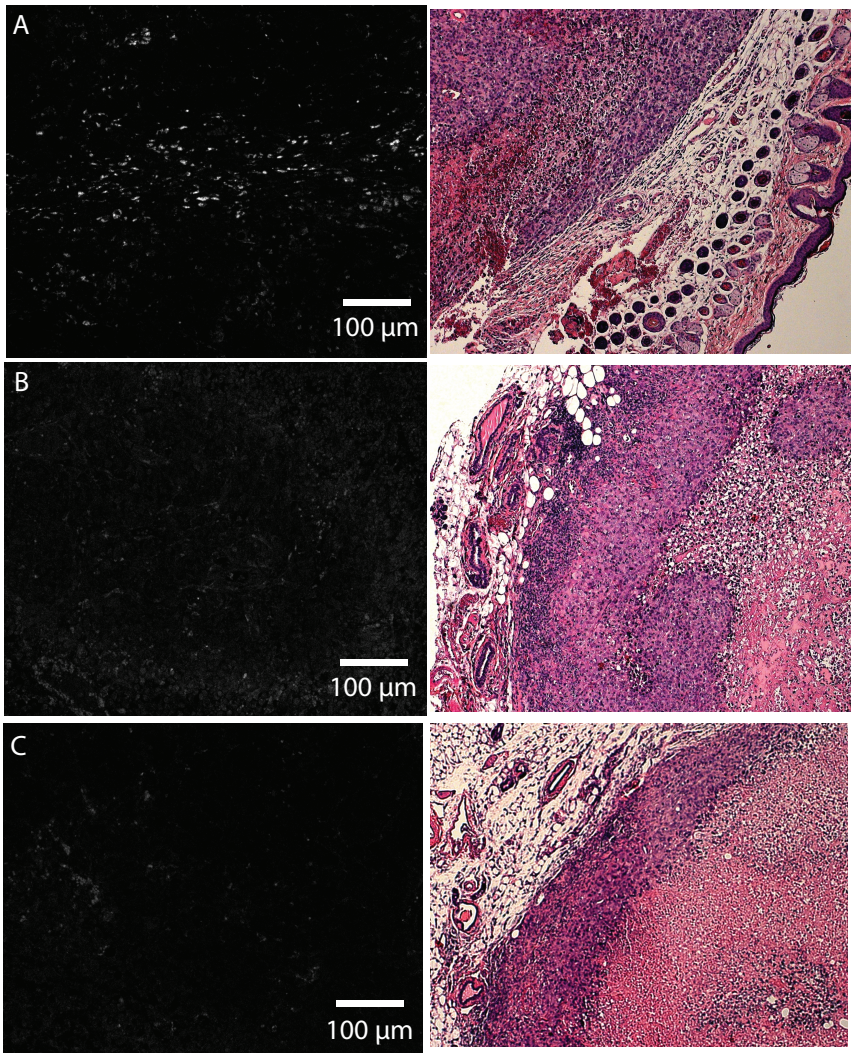

Figure 10S. Fluorescence and H&E of tumor histology. Increased levels of fluorescence by AlexaFluor 680 were observed for PA **1** (A) after 12 hours. PA **2** (B) and OEG-$K_2A_6K(C_{12})$ (C) did not show any fluorescence at the same timepoint. Representative H&E stains from different sections of the same tumors are shown to the right.

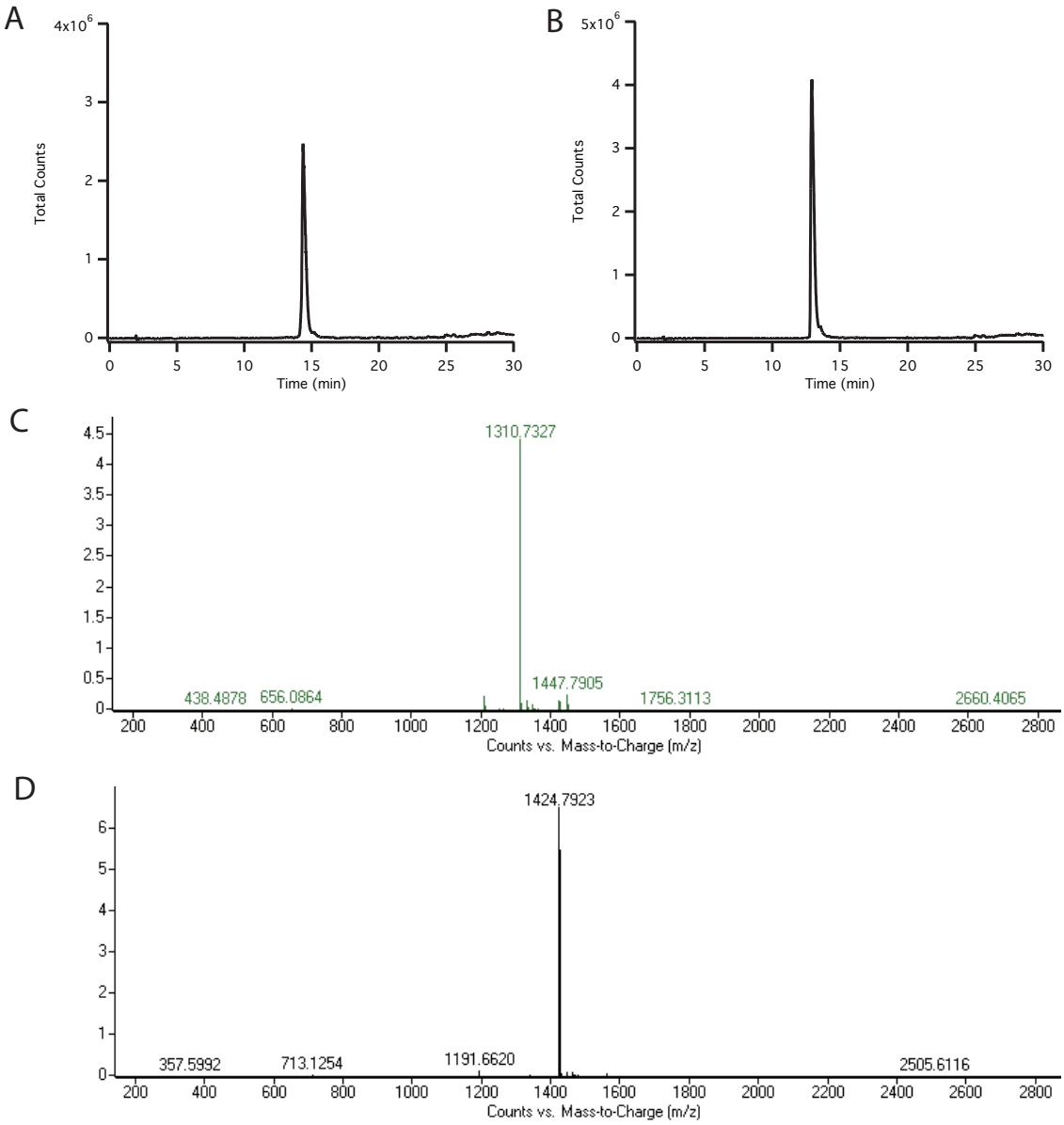

Figure 11S. LC-MS characterization. (A) HPLC trace of PA **1** using a gradient from 5% to 95% MeCN over 30 minutes. (B) HPLC trace of PA **2** using the same gradient. (C) ESI mass spec of PA **1** of the major peak shown in (A). (D) ESI mass spec of PA **2** from the major peak shown in (B).